Structural and magnetic disorder in $La_{1-x}Sr_xMnO_3$

2000 J. Phys.: Condens. Matter 12 4975

(http://iopscience.iop.org/0953-8984/12/23/307)

J. Phys.: Condens. Matter **12** (2000) 4975–4991. Printed in the UK PII: S0953-8984(00)10419-9

Structural and magnetic disorder in $La_{1-x}Sr_xMnO_3$

A Mellergård†, R L McGreevy‡ and S G Eriksson§

† Materials Physics, Royal Institute of Technology, S 100-44 Stockholm, Sweden
‡ Studsvik Neutron Research Laboratory, Uppsala University, S-611 82 Nyköping, Sweden
§ Inorganic Chemistry, Gothenburg University/Chalmers Technical University, S-412 96 Göteborg, Sweden

Received 16 December 1999, in final form 22 March 2000

Abstract. Total structure factors, that is both Bragg and diffuse scattering, have been measured for $La_{1-x}Sr_xMnO_3$ ($x = 0.2$ and 0.4) at temperatures between 15 and 1000 K by powder neutron diffraction using the SLAD diffractometer at the Studsvik Neutron Research Laboratory. The data have been used to simultaneously model the atomic and magnetic structures using the reverse Monte Carlo (RMC) method. The RMC models confirm that there are local lattice distortions, involving the O octahedra surrounding Mn ions, that disappear as T decreases through T_c (here defined as the point of inflexion of the net magnetic moment determined from Rietveld refinement, representing the onset of long range ferromagnetic order). The distortion referred to is *away* from the 'normal' Jahn–Teller distorted octahedron associated with Mn^{3+} and *towards* the more uniform octahedron associated with Mn^{4+}. It involves more than a single octahedron, so the correlation length is larger than ∼5 Å. The models are consistent with the proposal that the distortions occur around Mn^{4+} ions, though it is not possible to say whether the extra charge is localized on a single Mn. They may therefore be considered as lattice polarons. Both long range magnetic order (LRMO) and short range magnetic order (SRMO) increase rapidly as T decreases through T_c, but SRMO also persists above T_c. This is evidence for the existence of magnetic polarons above T_c. For the first time we show that the SRMO is correlated with the local lattice distortion, a higher ferromagnetic correlation being associated with shorter Mn–Mn distances. Lattice and magnetic polarons are therefore one and the same.

1. Introduction

Colossal magnetoresistance (CMR) materials have been known about for 40 years [1] but recently interest has been revived by the discovery that the CMR effect could be obtained in thin films of such materials [2], giving rise to the possibility of technological applications. Zener [3] suggested that ferromagnetism arises due to spin hopping between sites if the core spins of the initial and final states are sufficiently aligned. This type of interaction was termed double exchange. However, Millis *et al* [4, 5] have shown theoretically that double exchange alone is not sufficient to explain the extreme values of magnetoresistance that can be obtained, and have proposed that a strong electron–phonon coupling is also required. A number of proposals have been made for the origin of this coupling, including lattice polarons [6] and dynamic Jahn–Teller distortions [7].

The (time) average crystal structure of $LaMnO_3$ is the perovskite structure, but with a Jahn–Teller distortion of the oxygen octahedra surrounding Mn. Doping with either Ca or Sr in the region $x \sim 0.3$ produces an orthorhombic or rhombohedral structure with no long range Jahn–Teller distortion. Neutron powder diffraction (Bragg scattering) studies have shown evidence of small changes in the structure near the magnetic ordering temperature, T_c,

0953-8984/00/234975+17$30.00

for example variations in the lattice parameters [8], the mean square displacements of oxygen atoms [9] or the Mn–O bond lengths [10], which may be indicative of local structural distortions. However, the only techniques that have the possibility to directly probe the local atomic structure are total scattering, that is both Bragg and diffuse scattering, sometimes called pair distribution function (PDF) analysis, or EXAFS. Billinge *et al* [6] have studied $La_{1-x}Ca_xMnO_3$ by PDF analysis. They find that the second peak in the PDF, which is predominantly due to near neighbour O–O correlations, decreases in height rapidly as temperature increases through T_c. They have interpreted this as evidence of small polaron formation involving a uniform contraction of oxygen octahedra around Mn^{4+} ions above T_c. At low temperature, in the metallic state, all Mn ions have only the same average charge and so there is no local distortion. Louca *et al* [7], using precisely the same methodology but studying $La_{1-x}Sr_xMnO_3$, have found that the first peak in the PDF due to Mn–O correlations is split into two peaks at 1.95 and 2.25 Å (the second being smaller), which is interpreted as evidence of a strong local Jahn–Teller distortion. The same distortion appears to be evident both above and below T_c. However, Hibble *et al* [11] have recently reported the absence of such distinct local correlations in $La_{0.7}Sr_{0.3}MnO_3$ and $La_{1-x}Ca_xMnO_3$ ($x = 0.2, 0.3$); they only find broad wings at the tail of the first Mn–O PDF peak. Also, a distortion of this magnitude should be readily measurable by Mn EXAFS, but most EXAFS results [12–14] are interpreted in terms of a single near neighbour MnO distance. Some evidence has been found of a splitting [12] but the peaks are of similar intensity and at 1.83 and 2.06 Å, i.e. different from those found by Louca *et al* [7]. Small angle neutron scattering (SANS) results have been analysed in terms of a (magnetic) correlation length typically 10 Å or longer (for samples with large CMR behaviour) [15, 16]. More recent theory [17] suggests that the correlation length for the electron phonon coupling above T_c is much longer, of the order of 30 (cubic) lattice parameters; in this case one would not expect to see distinct correlations on a very local atomic scale.

The results appear at present to be rather inconsistent. If the local Jahn–Teller distortions persist below T_c then this seems incompatible with uniform oxygen octahedron contractions around T_c. EXAFS results do not really provide information on the contraction of oxygen octahedra, but the size of the Jahn–Teller distortion that has been proposed [7] should be quite easily observable by EXAFS. The correlation lengths from SANS are inconsistent with those suggested from PDF analysis. Further work is therefore required to clarify the situation.

In the present paper we report on a study of the local atomic and magnetic structures of $La_{1-x}Sr_xMnO_3$. The technique used is reverse Monte Carlo modelling of neutron powder diffraction data, including both Bragg and diffuse scattering [18, 19]. The technique has some similarities to the PDF method, but also some important differences. For example, this is the first time that the local magnetic structure has been considered; in previous work magnetic scattering has been ignored. In addition the data are interpreted in terms of full atomic and spin models which are consistent with all aspects of the data, not just in terms of parametric models based on particular features.

2. Experiment

The $La_{1-x}Sr_xMnO_3$ samples were prepared by solid state reaction from stoichiometric amounts of La_2O_3, $SrCO_3$ and MnO_2 in order to give the desired compositions. All starting materials had a purity of 99.9% or higher. Before use La_2O_3 was dried at 900 °C in a flow of O_2 for 12 hours. Batches of approximately 4 g were thoroughly mixed and milled, using ethanol as a grinding aid. In all sintering steps the samples were heated in air. In the first heat treatment they were fired as loose powders in Al_2O_3 crucibles at 950 °C for 12 hours. They were then fired in the form of pellets at 1100, 1200 and 1300 °C for 30, 80 and 100 hours

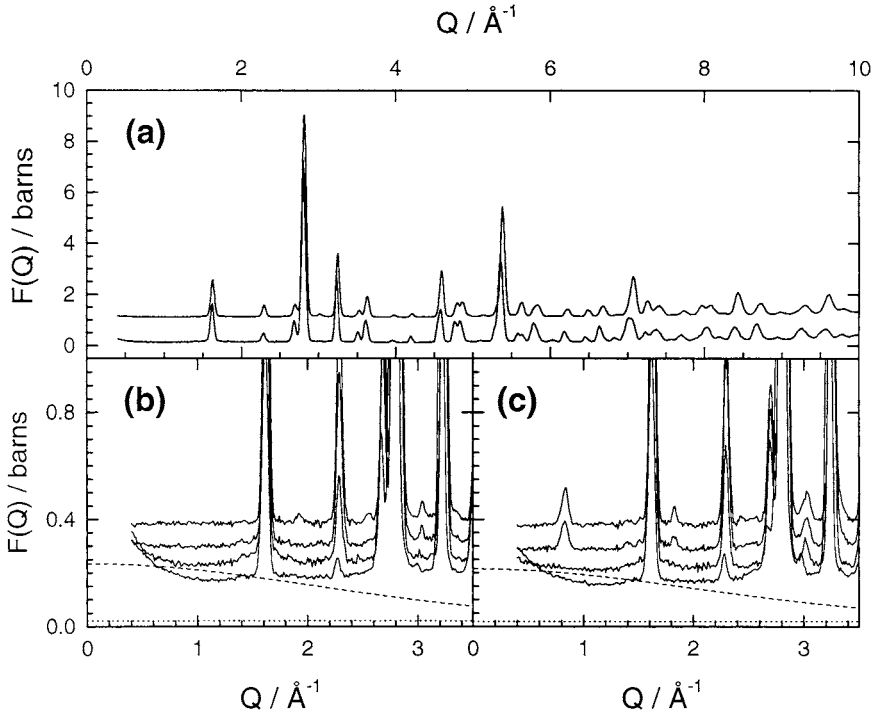

Figure 1. (a) Total structure factor, $F(Q)$, for $La_{1-x}Sr_xMnO_3$ at ambient temperature. $x = 0.2$ (lower curve) and 0.4 (upper curve), successive curves being offset by 1 for clarity. (b), (c) $F(Q)$ for $La_{1-x}Sr_xMnO_3$ at various temperatures, successively offset by 0.1 for clarity. (b) $x = 0.2$; $T = 900$ (lowest curve), 300, 200 and 15 K (uppermost curve). (c) $x = 0.4$; $T = 1000$ (lowest curve), 300, 150 and 100 K (uppermost curve). The incoherent scattering cross-section (dot) and the sum of the incoherent and theoretical paramagnetic scattering cross-sections (dash) are also shown. The peak widths show the instrumental resolution; there is no evidence of any sample dependent line broadening.

respectively. Between each sintering step the samples were reground and pelletized again. Before measurement the samples were reground.

Total structure factors, both Bragg and diffuse scattering, were measured for $La_{0.8}Sr_{0.2}MnO_3$ and $La_{0.6}Sr_{0.4}MnO_3$ at temperatures between 15 and 1000 K using the SLAD diffractometer at the Studsvik Neutron Research Laboratory [20, 21]. Measurements below and above ambient temperature used a closed cycle refrigerator and furnace respectively. The samples were contained in thin walled vanadium cylinders of 8 mm diameter. Separate measurements were made of the background, container and a vanadium standard. The sample data were corrected for background and container scattering, container absorption and sample self-absorption, multiple and inelastic scattering, and normalized to an absolute scale using standard procedures developed for studies of liquids and amorphous materials (see e.g. [22]). The structure factors for the two samples at ambient temperature are shown in figure 1(a)). Figures 1(b)) and 1(c)) show the low Q part at various temperatures. Two main points should be noted.

- The magnetic diffuse scattering can clearly be seen at the lowest Q and around the Bragg peak at $\sim$1.6 $Å^{-1}$, where it is most strongly peaked near T_c. In this paper we will define T_c to be the point of inflexion in the net magnetic moment, as determined from Rietveld

refinement (see section 3.1), representing the onset of long range (ferro)magnetic order. We estimate T_c as 310 ± 10 K for $x = 0.2$ and 350 ± 10 K for $x = 0.4$.

- At the highest temperatures the magnetic scattering is more sharply peaked towards low Q than predicted by the paramagnetic form factor, indicating that there is still significant short range magnetic order even at 3 T_c.

The measurements for $La_{0.8}Sr_{0.2}MnO_3$ were carried out on three separate occasions, one set below ambient temperature, one set just above and one set further above. It appears that there is a small difference in calibration for the middle set, which causes some relative errors in parameters derived later. However, the effect of these errors is generally clear and does not influence the data interpretation.

3. Data modelling

3.1. Rietveld refinement

The time average lattice and magnetic structures were refined from the Bragg scattering data by the Rietveld method using the FULLPROF program [23]. Refinements were carried out in both rhombohedral (space group $R\bar{3}c$) and orthorhombic (space group $Pnma$) unit cells. In the case of $La_{0.8}Sr_{0.2}MnO_3$ the rhombohedral cell was clearly the preferred one. Also, the results for $La_{0.6}Sr_{0.4}MnO_3$ were more consistent for $R\bar{3}c$ and these are reported here. The lattice parameters are very consistent with previously published results [24, 25] and show a small discontinuity in the variation of a around T_c. Figures 2(a)) and b) show the Mn–O bond length, d_{MnO} and the Mn–O–Mn bond angle. These are also found to be consistent with previous work. Figure 2(d)) shows the mean square oxygen displacement, $\langle u_O^2 \rangle$. It is found that for $La_{0.8}Sr_{0.2}MnO_3$ this decreases slightly more rapidly as T decreases through T_c, an effect which has been predicted theoretically and observed by others [4, 5, 9, 11]. A similar effect is not observed for $La_{0.6}Sr_{0.4}MnO_3$ where the CMR behaviour is weaker.

While the magnetic structure has been refined, the main purpose of this was to make an initial determination of the magnetic moment and to provide a starting point for RMC modelling. We have not yet attempted to analyse the average magnetic structure in detail and so no results will be reported here. The average moment is shown in figure 2(c)). At low T this is slightly higher than reported by others [25] but is consistent with the RMC model results (see below), which are consistent with both the magnetic Bragg and diffuse scattering as determined on an absolute scale, so we believe that the present result is accurate.

3.2. Reverse Monte Carlo (RMC) modelling

The instantaneous lattice and magnetic structures have been modelled by the RMC method using the RMCPOW program. This has been described in detail elsewhere [18, 19]. In Rietveld refinement the time average crystal structure of a material is represented by a set of parameters describing e.g. the lattice vectors, the average positions of atoms within the unit cell, thermal factors representing the average displacements of atoms from these average positions etc. These parameters are determined by fitting to a powder diffraction pattern, but using the elastic Bragg scattering data only. In RMCPOW the 'instantaneous' crystal structure is represented by a large configuration (model) containing thousands of atoms, typically that is tens or hundreds of individual unit cells. The configuration cell is therefore a supercell of the crystallographic unit cell. The positions of the individual atoms within the model are modified by random (Monte Carlo) processes in such a way as to improve the agreement between the diffraction pattern

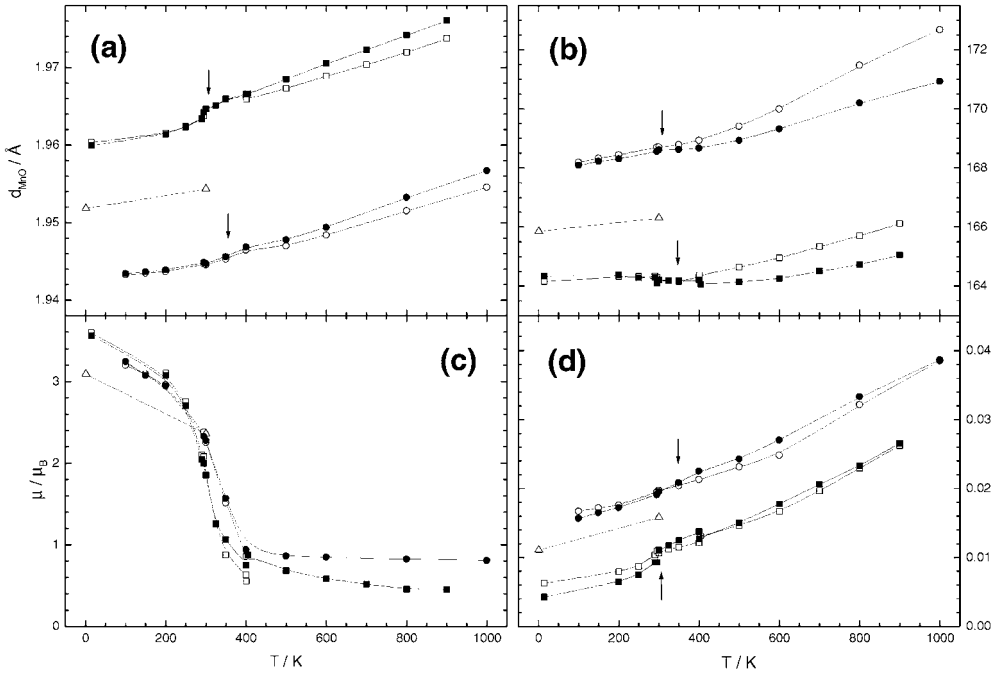

Figure 2. Parameters describing the average crystal structure, obtained by Rietveld refinement (open symbols) and from the RMC models (closed symbols). $La_{0.8}Sr_{0.2}MnO_3$ (squares), $La_{0.7}Sr_{0.3}MnO_3$ (up triangles) [25] and $La_{0.6}Sr_{0.4}MnO_3$ (circles). Vertical arrows indicate T_c. (a) Mn–O bond length; (d_{MnO}) (b) Mn–O–Mn bond angle; (c) net magnetic moment per Mn atom (μ) and (d) mean square displacements of O atoms, $\langle u_O^2 \rangle$, successively offset by 0.005 for clarity.

calculated from the model and that measured experimentally. However now the diffraction pattern includes both elastic scattering and (energy integrated) diffuse scattering.

Each model consisted of a supercell of $8 \times 8 \times 8$ rhombohedral crystal unit cells (i.e. 5120 atoms and 1024 spins), with periodic boundary conditions to obtain an effectively infinite system. The model dimensions were then fixed, with the initial lattice parameters being taken from the Rietveld refinement results. The initial atomic positions for the lowest temperature model were also taken from Rietveld refinement. The final configuration at each temperature was then taken as the starting point for modelling of data for the next highest temperature. In RMCPOW the total structure factor is calculated directly from the model, with the unit cell Bragg peaks representing the sample Bragg peaks and the (smoothed) supercell Bragg peaks representing the sample diffuse scattering (the experimental resolution is taken into account). Atoms and spins are moved/rotated by small random amounts in order to improve the fit between calculated and measured structure factors. The eventual result should be a model of the instantaneous atomic and magnetic structures that agrees with the data within experimental errors.

Figure 3 shows examples of the total structure factors and fitted models, with the fit split into its four separate components, i.e. atomic Bragg and diffuse scattering and magnetic Bragg and diffuse scattering. The quality of fit is comparable to that achieved by Rietveld refinement for the same data. Here it is useful to stress the differences between the methods. The Rietveld method fits the Bragg scattering only to refine an initial model of the (time) average structure within a single unit cell with a specified symmetry. The structure is defined

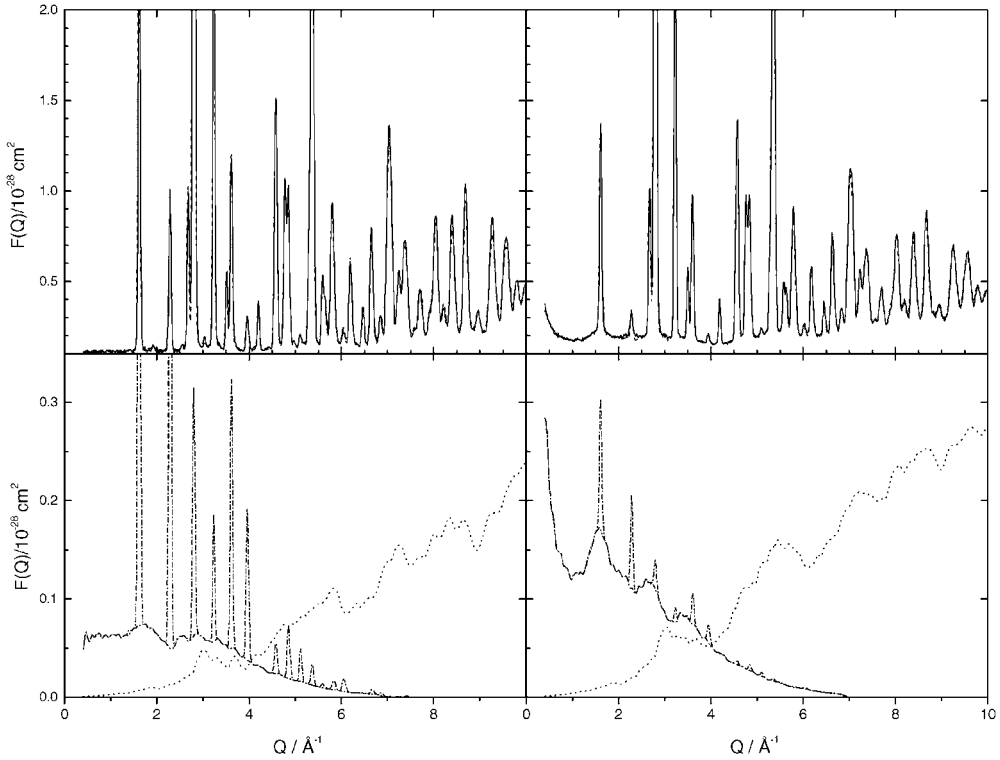

Figure 3. Total structure factors, $F(Q)$, for $La_{0.8}Sr_{0.2}MnO_3$ at 325 K (left) and 15 K (right). Experimental data (solid curve), RMC fit (dash curve), lattice diffuse scattering (dot curve), total magnetic scattering (dash–dot curve) and magnetic diffuse scattering (dash–dot–dot curve).

in terms of a relatively small number of parameters, e.g. cell constants, atomic positions and thermal factors, which are mathematically correlated but not (normally) subject to physical constraints. RMCPOW fits both the Bragg and diffuse scattering (in this case atomic and magnetic) to produce a model of the instantaneous structure defined in terms of individual atomic positions (and spins). The symmetry of individual unit cells is not defined, but only the shape of the overall model. The RMC model has many more parameters than Rietveld (i.e. 3×5120 parameters defining the atomic positions) and it might then be considered that any data set could be fitted since this is much larger than the number of data points (of order 1000). However, the RMC parameters are constrained and highly correlated, for example atoms have a finite size defined in terms of minimum atomic closest approach distances, which is why we do not in fact obtain a perfect fit to the data despite the high parameter/data ratio. In the present case the use of small atomic moves and appropriate fitting criteria also means that the resulting structure is a refinement of the initial structure, and not an independent determination of the structure.

Results for the average atomic structure within the unit cell from Rietveld refinement and RMC are compared in figure 2. In order to compare 'like with like' the average atomic distribution within the nominal unit cell in the RMC models has been subject to the same symmetry operations as the Rietveld models (this makes only a small difference). RMC and Rietveld results are very similar; some variation should be expected since RMC must be affected by the fact that both Bragg and diffuse scattering are fitted. The RMC models are slightly more

disordered at low T (this is a known feature of RMC methods) and the Rietveld models are slightly more disordered at high T (where Rietveld tends to couple resolution and thermal parameters but RMC is constrained by the modelling of both Bragg and diffuse scattering). The RMC models reproduce the small cusps in the d_{MnO} and $\langle u_O^2 \rangle$ at T_c for $La_{0.8}Sr_{0.2}MnO_3$. Therefore it may be considered that in terms of the average atomic structure within the unit cell the RMC models are consistent with previously published results.

4. Discussion

4.1. Atomic structure

While the consistency with Rietveld refinement has been stressed, RMC modelling has the advantage that one can also calculate local atomic correlations from the models. Figure 4 shows the partial pair correlation functions, $g_{ij}(r)$, for O–O and Mn–O pairs, and the total pair correlation function

$$G(r) = \sum_{i,j} c_i c_j b_i b_j (g_{ij}(r) - 1) \tag{1}$$

which is equivalent to the PDF as defined in various ways by other authors (e.g. 9, 10). c_i and b_i are the concentration and coherent neutron scattering length of atom type i. Note that Mn has a negative scattering length, so the first peak in $G(r)$ is negative. As T increases the first peaks in $g_{MnO}(r)$ and $g_{OO}(r)$ (due to near neighbour atoms) decrease in height and broaden, as would be expected. There is no evidence at any T of a separately resolved peak in $g_{MnO}(r)$ at 2.25 Å, as found by Louca *et al* [7], or of a peak at 1.83 Å as found from EXAFS by Tyson *et al* [12], though the wings do encompass both these distances. Good consistency is on the other hand found with the results of Hibble *et al* [11].

Figure 5 shows the mean positions, $\langle r_{ij} \rangle$, and variances, $\langle \sigma_{ij}^2 \rangle$ of the first peaks in $g_{MnO}(r)$ and $g_{OO}(r)$. If there were no correlations between the positions (motions) of neighbouring atoms these would be equal to the bond lengths, d_{ij}, and the sum of thermal parameters, $\langle u_i^2 \rangle + \langle u_j^2 \rangle$, as derived from the average crystal structure; in fact the results are rather close though $\langle \sigma_{ij}^2 \rangle$ are in general slightly larger. $\langle r_{MnO} \rangle$ and $\langle \sigma_{MnO}^2 \rangle$ for $x = 0.2$ clearly increase faster around T_c than would be expected from the slope of either the low or high T behaviour. $\langle r_{OO} \rangle$ shows only a very weak change at T_c. The behaviour of $\langle \sigma_{OO}^2 \rangle$ at T_c is harder to judge since this is somewhat affected by small calibration errors for a set of runs comprising four T points just above T_c. (O has the highest concentration and scattering length and hence ends up being most strongly coupled to the overall model dimensions. Small inconsistencies in the calibration at different angles can be accommodated by slight additional distortions in the oxygen structure.) However, from extrapolation of the high T behaviour it is clear that $\langle \sigma_{OO}^2 \rangle$ also shows an anomalous increase at T_c, larger than that for $\langle \sigma_{MnO}^2 \rangle$. The results for $x = 0.4$ (not shown) show no such obvious behaviour associated with T_c.

4.2. Magnetic structure

In order to model the magnetic structure we have used only a single value of the magnetic moment for all Mn ions. Below T_c, where the system is metallic, this is clearly valid (as a classical model). Above T_c it may be considered that we should use different moments for Mn^{3+} and Mn^{4+}. However, this really depends on the final conclusion of the study. If the lattice distortions are highly localized then this might be interpreted as evidence for different local charges. However, if the distortions, and hence the charge carriers, are distributed over several Mn sites then the average moment model is not a bad approximation. Given that the

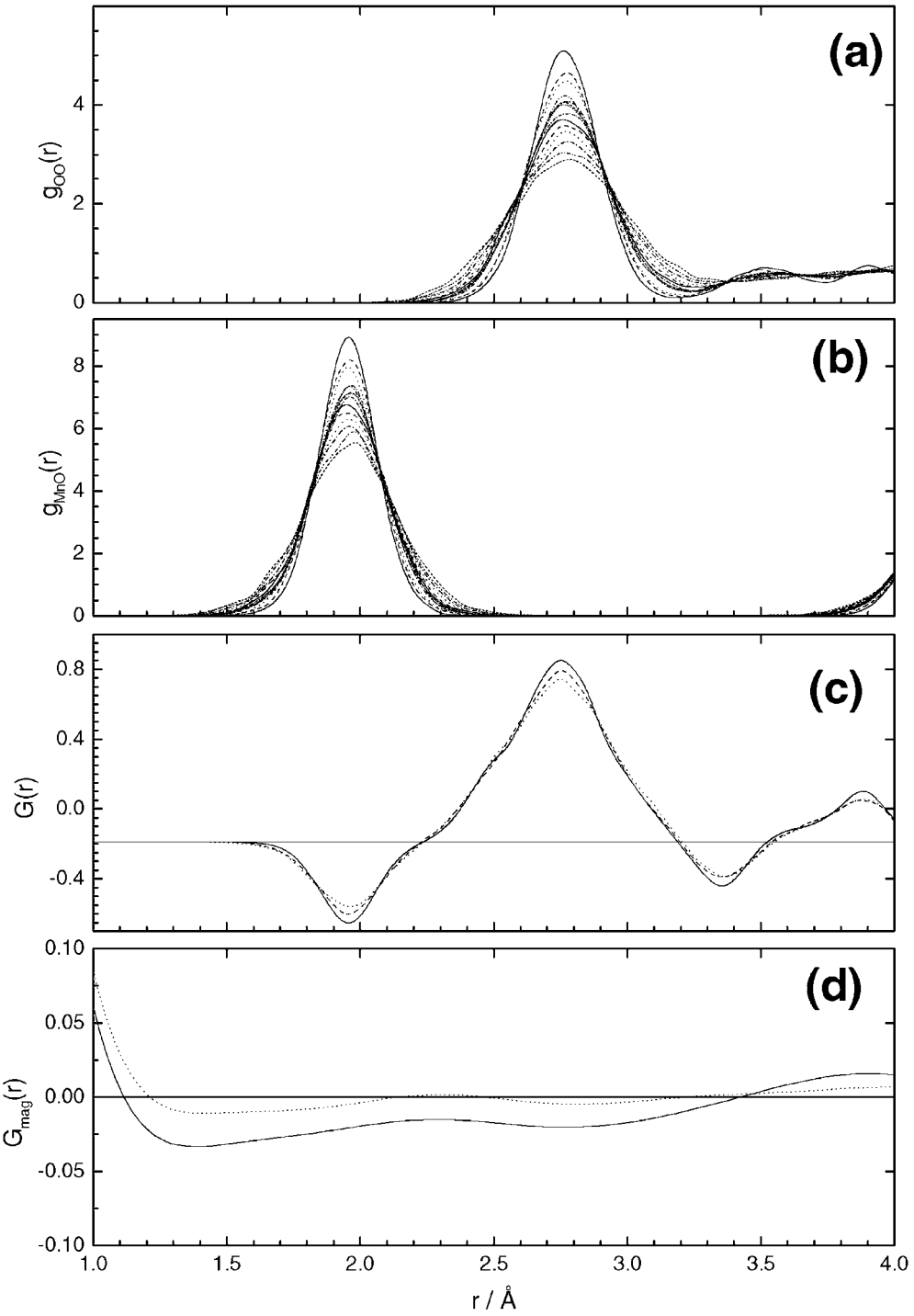

Figure 4. Pair correlation functions for $La_{0.8}Sr_{0.2}MnO_3$. (a) $g_{OO}(r)$ and (b) $g_{MnO}(r)$ at all temperatures measured. T increases as peak height decreases. (c) $G(r)$ at 15 K (solid curve), 250 K (dash curve) and 325 K (dot curve). (d) $G_{mag}(r)$ is the Fourier transform of the total magnetic structure factor (as shown in figure 3) at 15 K (solid curve) and 325 K (dot curve).

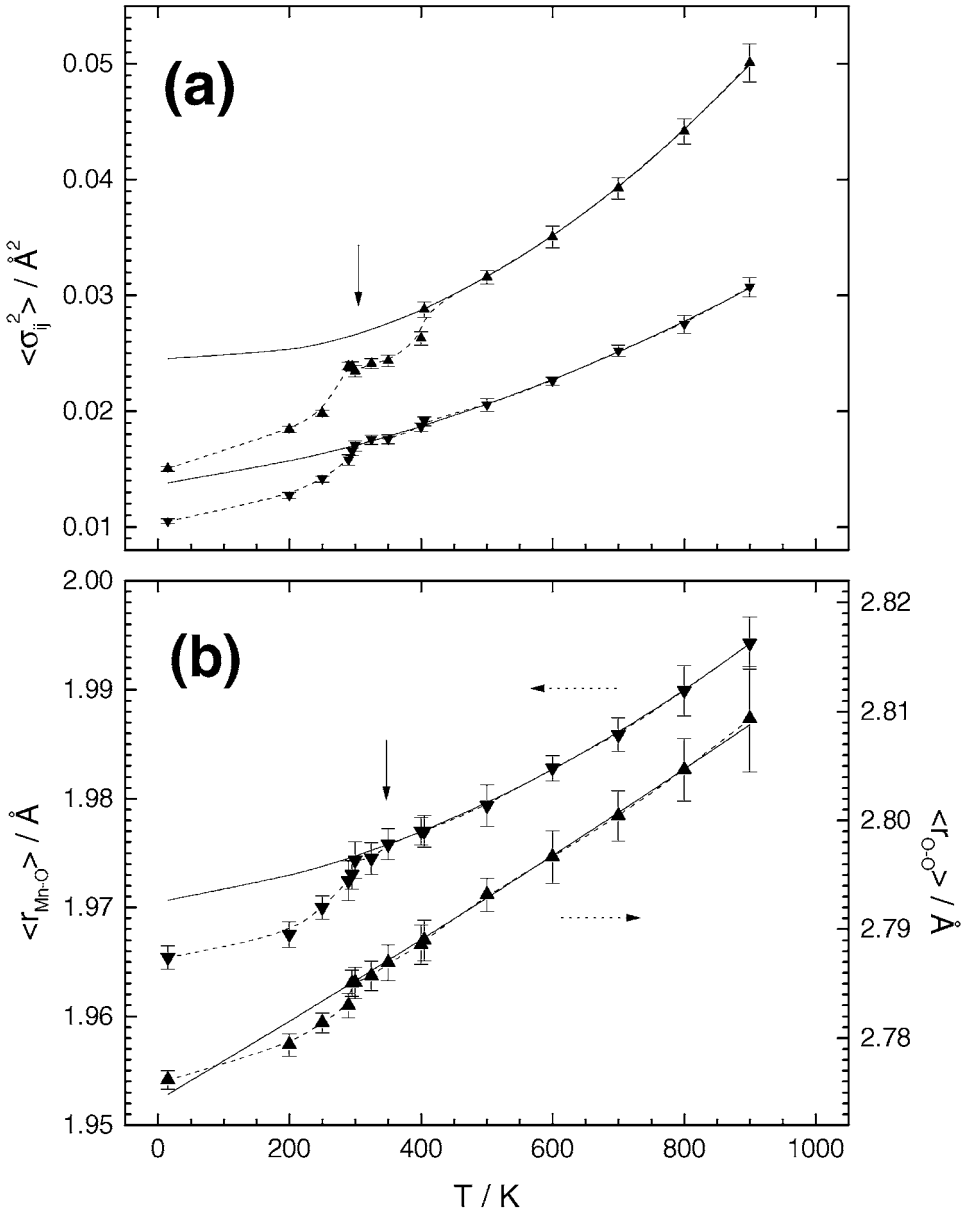

Figure 5. (a) Variance, $\langle\sigma_{ij}\rangle$, and (b) mean peak position, $\langle r_{ij}\rangle$, for the first peaks in $g_{OO}(r)$ (up triangle) and $g_{MnO}(r)$ (down triangle) for $La_{0.8}Sr_{0.2}MnO_3$. The dashed curves are spline fits to the data points. The solid curves are quadratic polynomial fits to the data points above T_c. Vertical arrows indicate T_c.

RMCPOW program can not yet deal with different moments that must be allowed to move between different magnetic sites, we have necessarily had to hope that an average moment model will suffice.

As noted earlier, we have not analysed the average magnetic structure in any detail. We can interpret the average atomic structure from the RMC model based on that derived from

Rietveld refinement. However, the magnetic unit cell may be doubled, for example, so it is not immediately obvious what basis to use. For $La_{0.6}Sr_{0.4}MnO_3$ at low T there is a magnetic scattering peak at $Q \sim 0.8$ Å^{-1} that could be consistent with an orthorhombic structure, but refining the lattice structure on this basis gives physically unrealistic thermal factors. In fact the magnetic diffuse scattering of the RMC model has managed to reproduce the integrated intensity of this peak, though not the narrow width (because of the inconsistency with the overall symmetry of the RMC model). This aspect of this type of RMC modelling requires further development.

Here we will concentrate on simple aspects of the change in magnetic structure through T_c. The average magnetic moment is shown in figure 2(c)); this agrees well with the results of Rietveld refinement. At high T we find that there remains a small net magnetization in the RMC models. The structure factors (figure 1) show that the magnetic diffuse scattering at high T is different from that expected for purely paramagnetic behaviour, indicating significant remaining short range magnetic correlations. It is possible that if these correlations are on a similar length scale to the RMC model there may be some finite size effect.

Figure 6 shows the spin–spin correlation function for $La_{0.8}Sr_{0.2}MnO_3$, that is the average angle (cosine) between spin pairs as a function of separation, $\langle \cos\theta(r) \rangle$. This is obviously only defined at separations where there are Mn atoms, so $g_{MnMn}(r)$ is also shown. $\langle \cos\theta(r) \rangle$ is almost flat at low T, indicating long range ferromagnetic order. The average value, ~0.61 for $x = 0.2$, implies an average projection relative to the net magnetization direction (i.e. the lattice) $\langle \cos\theta_l \rangle \sim (0.61)^{1/2} = 0.78$. This is consistent with the fact that for an average spin $S = 0.8 \times (4/2) + 0.2 \times (3/2) = 1.9$ we would expect $\langle \cos\theta_l \rangle = S/(S(S+1))^{1/2} = 0.81$. $\langle \cos\theta(r) \rangle$ is zero at high T at large r, indicating that there is no long range magnetic order (LRMO), but rises at low r indicating significant remaining short range magnetic order (SRMO). The SRMO appears to extend out to about 8–10 Å. Around T_c the large r value is finite and the low r rise remains, with perhaps a slightly longer correlation length. It should also be noted that at T_c and above there is a definite trend for the values of $\langle \cos\theta(r) \rangle$ within the first few individual peaks in $g_{MnMn}(r)$ to rise towards lower r, indicating a stronger ferromagnetic interaction for Mn–Mn pairs that are slightly closer.

As a measure of the LRMO we have used the average value of $\langle \cos\theta(r) \rangle$ between 16 and 18 Å, and as a measure of SRMO the average value corresponding to the first peak in $g_{MnMn}(r)$ (~3.9 Å). These are shown as a function of T in figure 7. Obviously both SRMO and LRMO show a clear transition at T_c. As noted above, the LRMO decreases to zero above T_c while the SRMO remains finite. The increase in magnetic order as T decreases through T_c almost exactly matches the decrease in lattice distortion. To illustrate this we also show in figure 7 the function

$$l(T) = 0.6\left(1 - \frac{\langle \sigma^2_{MnO}(T) \rangle - \langle \sigma^2_{MnO}(T) \rangle_{fit}}{\langle \sigma^2_{MnO}(T) \rangle - \langle \sigma^2_{MnO}(T) \rangle_{fit}}\right) \tag{2}$$

where *fit* indicates the appropriate solid curve in figure 5 (that is a quadratic polynomial fit to the high T behaviour of $\langle \sigma^2_{MnO}(T) \rangle$). The factor 0.6 is purely used for graphical scaling.

In the present case powder diffraction data provide no strong information on the magnetization direction below T_c relative to the lattice. We have tested this by rotating the whole magnetic structure and recalculating the structure factor, and find little change. This aspect should therefore be studied with single crystals.

4.3. CMR behaviour

We should now consider if we can derive a self-consistent explanation for the changes in lattice and magnetic structure in the RMC models. Firstly let us consider the lattice effects.

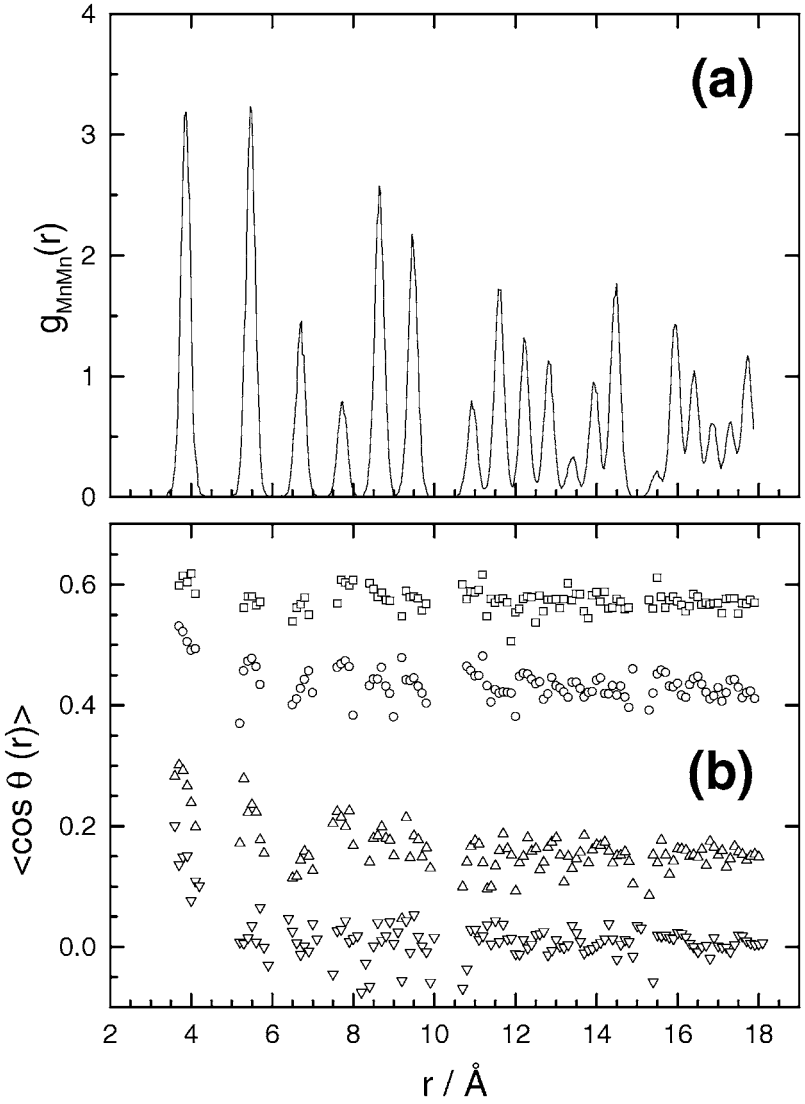

Figure 6. Spin correlation functions for $La_{0.8}Sr_{0.2}MnO_3$. (a) Pair correlation function, $g_{MnMn}(r)$, i.e. the function describing the positional correlations of spins. $T = 15$ K. (b) Average angle cosine between Mn–Mn spin pairs as a function of separation, $\langle \cos\theta(r) \rangle$, i.e. the function describing the angular correlation of spins. $T = 15$ (square), 200 (circle), 300 (up triangle) and 900 K (down triangle).

Imagine that a single Sr^{2+} is substituted for La^{3+} in $LaMnO_3$, thus injecting a single hole, and let us further assume that this hole is localized as a single Mn^{4+} ion. Because of the higher positive charge (compared to Mn^{3+}) this will attract the surrounding O^{2-} ions, producing a local lattice distortion. Note that the distortion referred to here is away from a Jahn–Teller distortion, which is the 'normal' situation in $LaMnO_3$, and *towards* a uniform octahedron. However, the more uniform octahedron is coupled with the rest of the lattice so there must be some strain field at longer distances. We would then expect to find Mn–O bond lengths within the Mn^{4+} octahedron that were slightly longer than expected for a 'pure' Mn^{4+} oxide (1.91 Å),

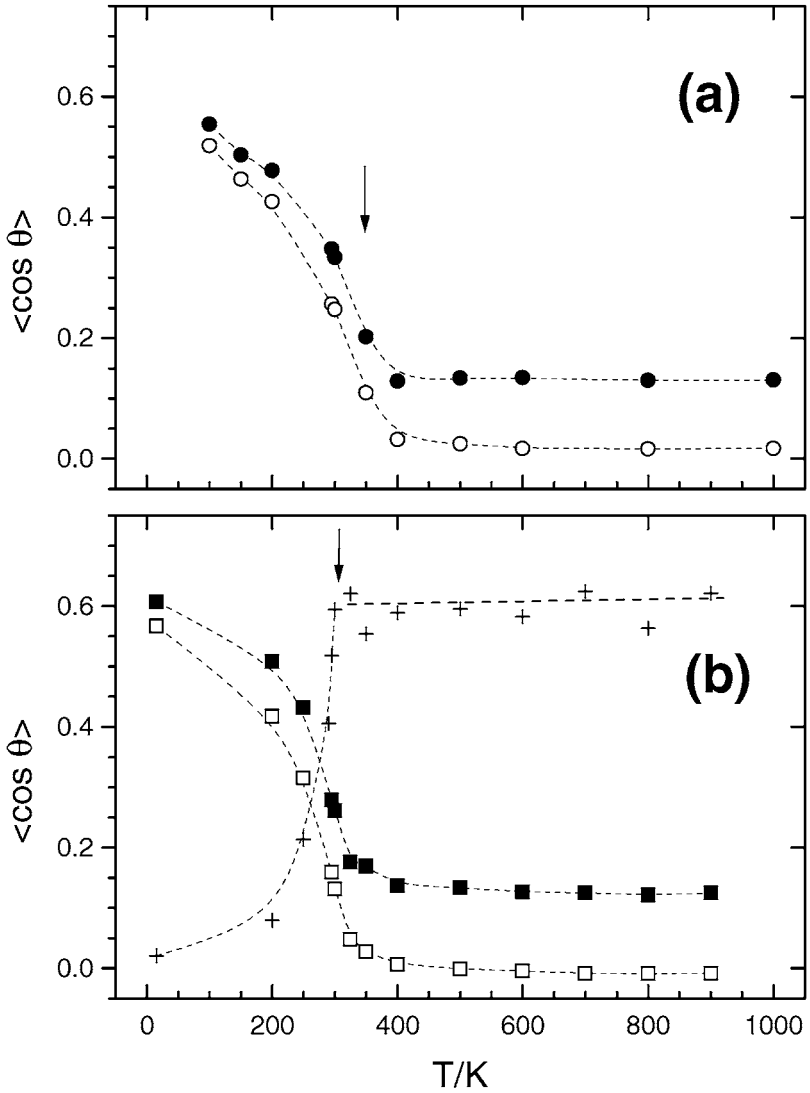

Figure 7. Parameters describing the short range magnetic order (SRMO) and long range magnetic order (LRMO) in (a) $La_{0.6}Sr_{0.4}MnO_3$ (circles) and (b) $La_{0.8}Sr_{0.2}MnO_3$ (squares). Open symbols: $\langle \cos\theta(16 < r < 18\ \text{Å})\rangle$ (LRMO). Solid symbols: $\langle \cos\theta(3 < r < 4.5\ \text{Å})\rangle$ (SRMO). The crosses show the function $l(T)$ (equation (2)) describing the local lattice distortion. Lines are guides to the eye. Vertical arrows indicate T_c.

and in the surrounding octahedra bond lengths slightly shorter and longer than expected for $LaMnO_3$ (1.925 and 2.225 Å). There will therefore be a range of Mn–O bond lengths between ∼1.9 Å and 2.25 Å, not just bond lengths due to Mn^{4+}–O and Mn^{3+}–O.

As more Sr^{2+} is added, the distribution of Mn^{4+} will be determined by a number of competing factors. Coulomb repulsion will tend to separate Mn^{4+}, but the strain fields will be reduced if they cluster. There will be some preference for Mn^{4+} to be in the vicinity of the (static) Sr^{2+} defects. These charge (i.e. electronic) effects will of course couple to the magnetic interactions. If reduction of the strain field strongly dominates, and Mn^{4+} cluster,

then different bond lengths for Mn^{3+}–O and Mn^{4+}–O might be resolved in $g_{MnO}(r)$. However, if Coulomb repulsion dominates then there will be a whole range of bond lengths in between those for Mn^{3+}–O and Mn^{4+}–O and $g_{MnO}(r)$ will be a single broad peak—this latter situation is consistent with our models (and the data of Billinge *et al* [6] and Hibble *et al* [11]). If holes hop rapidly through the lattice at high T then this motion will lead to additional blurring of the bond length distribution. It should also be noted that at particular x the competing interactions could lead to particular geometrical ordering, e.g. Mn^{3+}–Mn^{4+} charge ordering at $x = 0.5$.

Given a random distribution of Mn^{4+} (not the same as a uniform distribution) we expect a situation at $x \sim 0.2$ where the strain fields of all the Mn^{4+} overlap and form a percolating network (the bond percolation threshold for a cubic lattice is 0.25). Given self-similarity arguments this would actually be independent of the precise extent of the strain field if the overall symmetry is close to cubic. The LRO of the Mn^{3+} Jahn–Teller distorted octahedra will then be broken, leading to a transition in the crystallographic symmetry from orthorhombic to rhombohedral. This is precisely what is observed.

In the discussion above we have started from the premise that the holes (Mn^{4+}) are localized, i.e. the sample is an insulator at low T and may exhibit polaronic conduction at high T due to hopping of holes (and their accompanying lattice distortions). However, if we alternatively assume that the holes are completely delocalized, i.e. the system is metallic/semiconducting, then each Mn will have only some average charge dependent on x—hence there will be a single average $Mn^{(3+x)+}$–O bond length broadened by normal thermal vibrations. In this case the width of the peak in $g_{MnO}(r)$ will be narrower relative to the case for localized holes. This is precisely what is observed as T decreases through T_c for $x = 0.2$, that is $\langle\sigma^2_{MnO}\rangle$ decreases at the insulator–metal transition. $\langle r_{MnO}\rangle$ changes only slightly since the macroscopic charge balance does not change at T_c, only the local charge balance. Although the discussion has so far concentrated on $\langle\sigma^2_{MnO}\rangle$ we would also expect a change in $\langle\sigma^2_{OO}\rangle$. In fact $\Delta\langle\sigma^2_{OO}\rangle^{1/2}/\langle r_{OO}\rangle \approx \Delta\langle\sigma^2_{MnO}\rangle^{1/2}/\langle r_{MnO}\rangle$ (where Δ indicates the 'anomalous' change through T_c), as would be expected from simple geometrical arguments.

From the above arguments we can conclude that the RMC models are consistent with the idea that conduction in $La_{1-x}Sr_xMnO_3$ at high T is due to polaron hopping. The 'size' of the polaron is certainly larger than a single Mn–O octahedron since, as indicated, the strain field must be more widely distributed. Because of the distribution of bond lengths in the strain field, and the electron–lattice coupling, one would expect some spreading of the local charge distribution, though this may depend on the coupling to the spin state. At the highest T we have found that the low Q diffuse magnetic scattering is still distinctly different from the expected paramagnetic form factor (figure 1). It is impossible to obtain any reliable functional fit (e.g. Lorentzian) to the shape of the low Q magnetic scattering (the lowest Q value is too large), but we have checked that our results are consistent with the SANS results of De Teresa *et al* [15, 16] which show a correlation length of the order of 6 Å at $T = 4\ T_c$ for $(La_{0.75}Tb_{0.25})_{0.75}Ca_{0.25}MnO_3$; this is also consistent with the low r behaviour of $\langle\cos\theta(r)\rangle$ as shown in figure 6. Lynn *et al* [26] have derived a correlation length of the order of 10 Å for $La_{0.67}Ca_{0.33}MnO_3$ at $T = T_c$ based on quasi-elastic neutron scattering from spin fluctuations. We therefore conclude that a 'typical' polaron involves *at least* one Mn–O octahedron and its six nearest neighbour octahedra, and that this is both a lattice and a magnetic polaron [27] (i.e. involving a lattice distortion due to the additional local charge and short range magnetic order).

Most of the evidence for identifying a lattice and a magnetic polaron as one coherent 'object' is indirect, although nevertheless convincing. For $x = 0.2$ the fractional change in $\langle\sigma^2_{MnO}\rangle$ through T_c is $\sim 1/3$, i.e. the 'normal' thermal vibrations are larger than the polaronic distortion, so it is difficult to unambiguously 'find' a lattice polaron within the RMC model.

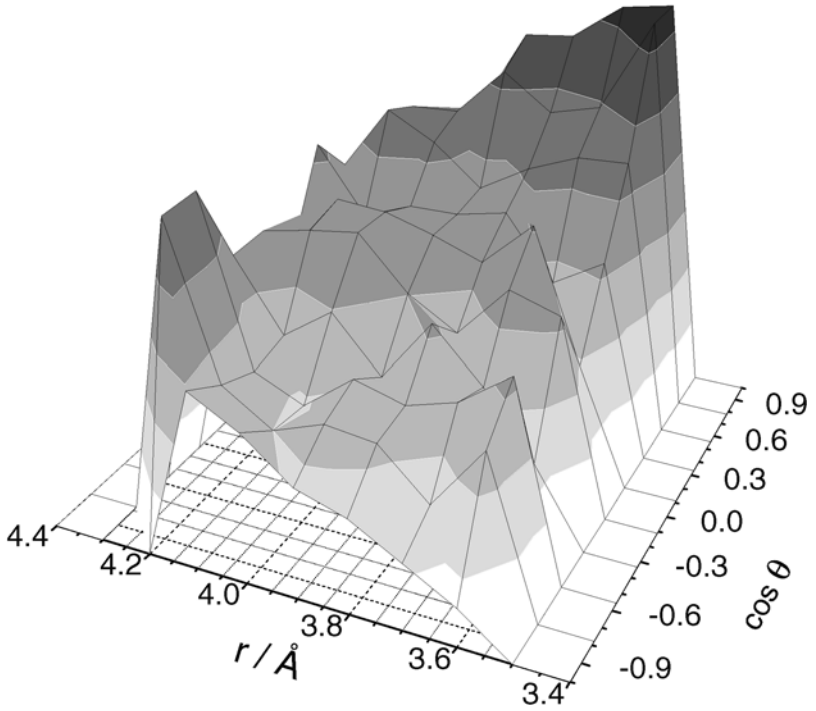

Figure 8. Spin–spin angle distribution function $p(\cos\theta(r), r)$ for $La_{0.8}Sr_{0.2}MnO_3$ at 325 K. Only distances corresponding to Mn–Mn near neighbours, $3.4 < r < 4.4$ Å, are shown.

Hence it is also difficult to directly correlate the SRMO around an individual spin with the local atomic arrangement; we would need considerably better statistics and to know what particular many body correlation function to calculate. However, direct evidence comes from the slope of $\langle\cos\theta(r)\rangle$ at distances within the first peak of $g_{MnMn}(r)$ (figure 6). The fact that for T_c and above $\langle\cos\theta(r)\rangle$ is clearly higher (despite the poor statistics) at 3.5 Å than at 4.2 Å indicates that on average local spin clusters with a higher degree of SRMO occupy slightly less volume, which is consistent with a local lattice contraction around Mn^{4+}. We reiterate here that the distortion referred to is *away* from the 'normal' Jahn–Teller distorted octahedron associated with Mn^{3+} and *towards* the more uniform octahedron associated with Mn^{4+}.

Figure 8 shows the full $(\cos\theta(r))$ distribution for near neighbour Mn atoms in $La_{0.8}Sr_{0.2}MnO_3$ at 325 K (near T_c). The main peak occurs at short distances and close to $\cos\theta = 1$, i.e. ferromagnetic ordering. However, there is also clearly a weaker peak at longer distances close to $\cos\theta = -1$, i.e. antiferromagnetic ordering. This is consistent with a situation where the coupling is antiferromagnetic around lower charge cations, e.g. Mn^{3+}, and ferromagnetic around higher charge cations, e.g. Mn^{4+}, and the Mn–O bond length is reduced around the higher charge cations.

Application of a magnetic field to samples with $x \sim 0.17$ at ambient temperature can cause a transition from the (low T, zero field) orthorhombic structure to the (high T, zero field) rhombohedral structure [28, 29]. At constant T the same transition also occurs as a result of increasing x, i.e. increasing the average Mn charge. This is consistent with our results. Application of a magnetic field would tend to align spins and hence, via the spin–lattice coupling (as shown in figure 8) decrease the local Mn–O bond length, equivalent to increasing the Mn charge.

4.4. Consistency with other work.

In the interpretation of their PDF Louca *et al* [7] have used only three parameters; these are the positions of the peaks observed in $G(r)$ at ∼1.95 and ∼2.25 Å and the area of the 1.95 Å peak, but not that of the 2.25 Å peak (the latter overlapping with O–O and La–O contributions). The peak positions are interpreted as showing two distinct bond lengths in Jahn–Teller distorted O octahedra, with the area of the first peak then giving information on the number of such distorted octahedra. The peak positions change slightly with composition/temperature but this has not been interpreted. For $x = 0$ the Mn–O coordination at 1.95 Å is ∼4, implying a coordination of 2 at 2.25 Å. This is the expected result if all Mn ions are Mn^{3+}, i.e. four shorter and two longer Mn–O bonds per octahedron. At $x = 0.4$ the coordination at 1.95 Å is ∼6, implying a disappearance of all distorted octahedra. The fact that the same lattice distortion is observed both above and below T_c is referred to by the authors themselves as 'peculiar behaviour'.

If our $G(r)$ is integrated over the same r ranges as the PDF of Louca *et al* [7] then the coordination numbers derived are very similar, even though we do not resolve separate peaks at 1.95 and 2.25 Å. It might be argued that this lack of resolution is due to the fact that our Q range (10 $Å^{-1}$) is significantly shorter than that of Louca *et al* [7] (40 $Å^{-1}$), giving reduced real space resolution. However, this does not hold since we have used an inverse method of analysis, and we have fully treated the Q space resolution (which also has a detrimental effect on real space resolution), whereas Louca *et al* [7] have not. In addition the width of the peak in our $g_{MnO}(r)$ is consistent with Rietveld refinement (both our results and those of other workers).

There are a number of signs that suggest that in fact the resolution of a separate peak at ∼2.25 Å in the PDF of Louca *et al* [7] is due to some form of Fourier transform truncation effect, arising from either small systematic or statistical errors (we have confirmed this possibility by numerical tests). Firstly the width of the PDF peaks is slightly narrower than would be expected just from the Q range, without even including thermal effects. Secondly there are also, in some cases, peaks/shoulders resolved at ∼1.8 Å, i.e. on the opposite side of the main (1.95 Å) peak and at ∼2.15 Å, and these are both positive (which should be physically impossible given the negative scattering length of Mn) and of similar magnitude to the 2.25 Å peak. Finally the PDFs of Hibble *et al* [11] for $La_{1-x}Sr_xMnO_3$, obtained from pulsed neutron data ranging out to 50 $Å^{-1}$, do not show any distinct peak at 2.2 Å. Instead their data show wings similar to our results.

The RMC models seem quite consistent with the PDFs of Billinge *et al* [6], though their results are for Ca doping rather than Sr doping so some differences might be expected (Ca doping produces a larger CMR effect). For example, we find that $\langle\sigma^2_{OO}\rangle$ for (Sr) $x = 0.2$ changes by ∼30% through T_c, while they conclude a width change of ∼20% from the change in the second peak height of the PDF for (Ca) $x = 0.21$ (but note that $G(r)$ also has a contribution from $g_{LaO}(r)$ at this distance). Their interpretation of this result in terms of a uniform contraction of O octahedra around Mn^{4+} ions, of the order of 0.1 Å O displacement, is not inconsistent with the changes in our models if it is viewed as some form of average representation of the structural change.

Another factor that should be considered is magnetic scattering. Billinge *et al* [6] and Louca *et al* [7] have assumed that the transform of the magnetic scattering will only contribute at higher r, around the position of the first peak in $g_{MnMn}(r)$ (3.9 Å). However, because of the magnetic form factor, the magnetic scattering contributes at all r. From the RMC models we can calculate the magnetic scattering intensity in Q space, and hence are able to perform a direct Fourier transform to r space; the results are shown in figure 5. The change in the

amplitude of $G_{mag}(r)$ with temperature at 1.95 and 2.75 Å is ∼10% of the change in peak height of $G(r)$. While this introduces a small, though not insignificant error it should be noted that the apparent change in magnetic scattering contribution can be significantly increased if the minimum Q value of the original data is higher, e.g. ∼1 Å^{-1}. Note that $G_{mag}(r)$ is not in itself a physically meaningful correlation function because of the Q dependence of the magnetic form factor and the vector nature of the magnetic moment; it is simply the direct Fourier transform of the magnetic contribution to the structure factor. For this reason $G_{mag}(r)$ is non-zero at small r, for example.

It is not so straightforward to compare our results with those of EXAFS since the methods of analysis are somewhat different [12–14]. However, two points can be noted. The shape of the first peak in $g_{MnO}(r)$ is not exactly Gaussian, particularly above T_c. It would therefore be possible to interpret this as indicating more than one Mn–O distance by fitting of one or more Gaussians. Secondly any EXAFS analysis may be complicated by the fact that the electronic state of the Mn ions is clearly coupled to the local atomic arrangement, and hence the EXAFS signal will be determined by a convolution of both these effects. This may lead to misleading results if a single electronic state is actually assumed.

5. Conclusions

The first point to be made is that the RMC configurations, i.e. the atomic coordinates and spin vectors, are obtained directly from modelling of the experimental data. The results are therefore entirely independent of any prior information or view of how the system 'should' behave. In interpreting the configurations we have also tried to be as independent as possible. Our conclusions (for $x = 0.2$ and 0.4) are as follows:

- Our results and RMC models are consistent with other crystallographic studies (e.g. [24, 25]) in terms of the time average crystal structure, and the PDF results of Billinge *et al* [6] and Hibble *et al* [11] in terms of the local structure.
- The RMC models confirm that there are local lattice distortions, involving the O octahedra surrounding Mn ions, that disappear as T decreases through T_c. The distortion referred to is *away* from the 'normal' Jahn–Teller distorted octahedron associated with Mn^{3+} and *towards* the more uniform octahedron associated with Mn^{4+}.
- The distortion is found to involve more than a single octahedron, so the correlation length is larger than ∼5 Å.
- The models are consistent with the proposal that the distortions occur around Mn^{4+} ions, though it is not possible to say if the extra charge is localized on a single Mn. They may therefore be considered as lattice polarons,
- Both LRMO and SRMO increase rapidly as T decreases through T_c, but SRMO also persists above T_c. This is evidence for the existence of magnetic polarons above T_c.
- The SRMO is correlated with the local lattice distortion, with evidence that a ferromagnetic correlation is associated with shorter Mn–Mn distances and antiferromagnetic correlation with longer distances. Lattice and magnetic polarons are therefore one and the same.

While many of these effects have also been concluded by other authors, this is the first time that they have been combined into a single model, and the first time that direct evidence has been obtained for the coupling of lattice and magnetic polarons. The results suggest that it would be interesting to extend the study of this coupling both to lower x, where the system is no longer metallic at low T, and to the region around the ferromagnetic–antiferromagnetic transition at $x = 0.5$.

Acknowledgments

This work has been supported by the Swedish Natural Sciences Research Council (NFR). AM thanks KTH for continuous support.

References

[1] Jonker H H and van Santen J H 1950 *Physica* **16** 337
[2] von Helmolt R, Wecker J, Holzapfel B, Schultz L and Samwer K 1993 *Phys. Rev. Lett.* **71** 2331
[3] Zener C 1951 *Phys. Rev.* **82** 403
[4] Millis A J, Shraiman B I and Mueller R 1996 *Phys. Rev. Lett.* **77** 175
[5] Millis A J, Littlewood P B and Shraiman B I 1995 *Phys. Rev. Lett.* **74** 5144
[6] Billinge S J L, DiFrancesco R G, Kwei G H, Neumeier J J and Thompson J D 1996 *Phys. Rev. Lett.* **77** 715
[7] Louca D, Egami T, Brosha E L, Rödear H and Bishop A R 1997 *Phys. Rev.* B **56** R4875
[8] Radaelli P G, Cox G E, Marezio M, Cheong S-W, Schiffer P E and Ramirez A P 1995 *Phys. Rev. Lett.* **75** 4488
[9] Dai P, Zhang J, Mook H A, Liou S-H, Dowben P A and Plummer E W 1996 *Phys. Rev.* B **54** R3694
[10] Argyriou D N, Mitchell J F, Potter C D, Hinks D G, Jorgensen J D and Bader S D 1996 *Phys. Rev. Lett.* **76** 3826
[11] Hibble S J, Cooper S P, Hannon A C, Fawcett I D and Greenblatt M 1999 *J. Phys.: Condens. Matter* **11** 9221
[12] Tyson T A, Mustre de Leon J, Conradson S D, Bishop A R, Neumeier J J, Röder H and Zeng J 1996 *Phys. Rev.* B **53** 13 985
[13] Subías G, García J, Blasco J and Proietti M G 1998 *Phys. Rev.* B **57** 748
[14] Booth C H, Bridges F, Kwei G H, Lawrence J M, Cornelius A L and Neumeier J J 1998 *Phys. Rev.* B **57** 10 440
[15] De Teresa J M, Ibarra M R, Algarabel P A, Ritter C, Marquina C, Blasco J, García J, del Moral A and Arnold Z 1997 *Nature* **386** 256
[16] De Teresa J M, Ritter C, Ibarra M R, Algarabel P A, García-Muñoz J L, Blasco J, García J and Marquina C 1997 *Phys. Rev.* B **56** 3317
[17] Sheng L, Xing D Y, Sheng D N and Ting C S 1997 *Phys. Rev. Lett.* **79** 1710
[18] Mellergård A and McGreevy R L 1999 *Acta Crystallogr.* A, at press
[19] Mellergård A and McGreevy R L 1998 *J. Phys.: Condens. Matter* **10** 9401
[20] Wannberg A, Delaplane R G and McGreevy R L 1997 *Physica* B **234–236** 1155
[21] Wannberg A, Mellergård A, Zetterström P, Delaplane R G, Grönros M, Karlsson L-E and McGreevy R L *J. Neutron Res.* **8** 133
[22] Egelstaff P 1987 *Neutron Scattering (Methods of Experimental Physics 23B)* ed K Skold and D Price (New York: Academic)
[23] ftp://charbyde.scalay.cea.fr/pub/divers/fullp/
[24] Mitchell J F, Argyriou D N, Potter C D, Hinks D G, Jorgensen J D and Bader S D 1996 *Phys. Rev.* B **54** 6172
[25] Radaelli P G, Iannone G, Marezio M, Hwang H Y, Cheong S-W, Jorgensen J D and Argyriou D N 1997 *Phys. Rev.* B **56** 8265
[26] Lynn J W, Erwin R W, Borchers J A, Huang Q, Santoro A, Peng J-L and Li Z Y 1996 *Phys. Rev. Lett.* **76** 4046
[27] Clausen K N, Hayes W, Keen D A, Kusters R M, McGreevy R L and Singelton J 1989 *J. Phys.: Condens. Matter* **1** 2721
[28] Asamitsu A, Moritomo Y, Tomioka Y, Arima T and Tokura Y 1995 *Nature* **373** 409
[29] Kamenev K V, McIntyre G J, McK Paul D, Lees M R and Balakrishnan G 1998 *Phys. Rev.* B **57** R6675